Sustainable Energy & Fuels

ROYAL SOCIETY OF CHEMISTRY

PAPER

Cite this: *Sustainable Energy Fuels*, 2020, **4**, 5818

A techno-economic perspective on solar-to-hydrogen concepts through 2025†

Thomas Grube, *[a] Julian Reul, [a] Markus Reuß, [a] Sonya Calnan, [b] Nathalie Monnerie, [c] Rutger Schlatmann, [b] Christian Sattler, [c] Martin Robinius [a] and Detlef Stolten [ad]

The transition towards a renewable energy-based society is challenged by spatial and temporal imbalances of energy demand and supply. Storage properties and versatility may favor hydrogen to serve as the linking element between renewable energy generation and a variety of sector coupling options. This paper examines four alternative solar-based hydrogen production concepts based on concentrated solar (CSP) or photovoltaic (PV) power generation and solid oxide (SOE) or polymer electrolyte membrane (PEM) electrolysis, namely, CSP-SOE and CSP-PEM, as well as PV-PEM concepts with (PV-PEM I) or without (PV-PEM II) power converters coupling both devices. In this paper, we analyze these concepts in terms of their techno-economic performance in order to determine the levelized cost of hydrogen (LCOH) for the target year 2025, based on different locations with different climate conditions. The analysis was carried out using a broadly applicable computer model based on an hourly resolved time-series of temperature and irradiance. The lowest LCOH was identified in the case of the CSP-SOE and CSP-PEM concepts with 14–17 €-ct per kW per h at high-irradiance locations, which clearly exceed the US Department of Energy (DOE) target of 6 $-ct per kW per h for the year 2020. Moreover, CSP-SOE also shows the highest hydrogen production volumes and, therefore, solar-to-hydrogen efficiencies. Considering the PV-PEM concepts, we found that the application of power converters for the electrical coupling of PV modules and electrolyzers does not contribute to cost reduction due to the higher related investment costs. A further system optimization is suggested regarding the implementation of short-term energy storage, which might be particularly relevant at locations with higher fluctuations in power supply.

Received 18th June 2020
Accepted 24th September 2020

DOI: 10.1039/d0se00896f

rsc.li/sustainable-energy

1 Introduction

The extensive implementation of renewable energy technologies is seen by many as the means to achieve a cleaner and more sustainable energy future. Renewable energy (RE) sources such as wind and solar radiation are, by their nature, fluctuating and, therefore, make securing a reliable energy supply more challenging. A possible solution to this is the production of hydrogen that could be cost-effectively stored and subsequently used in a great variety of applications. The sector coupling concept of transferring REs or RE-derived feedstocks to other sectors largely builds on the production of hydrogen for subsequent utilization in the transport, industrial or residential sectors.[1–3] In addition to wind power-based concepts, electrolytic hydrogen production using solar radiation may offer a promising alternative. However, renewable energy yields are strongly dependent on local solar irradiation levels and diverse technical concepts are presently available at different levels of maturity. The main focus of this study is the analysis of the techno-economic potential of electrolytic hydrogen production *via* different solar radiation-based pathways for the year 2025. The pathway alternatives considered here range from photovoltaic power generation connected to polymer electrolyte membrane (PEM) electrolysis, to concentrated solar power (CSP) combined with PEM or solid oxide electrolysis (SOE). This study builds on our previous publication by Reuß *et al.* (2019)[4] that focused on a technical assessment of solar hydrogen production systems comprising PV power generation and PEM electrolysis. The methodical approach to model-based assessment in this study was, initially, to further develop the required subsystem modules based on our previous work: PV and CSP-based power generation, as well as electrolytic hydrogen

[a]*Forschungszentrum Jülich GmbH, IEK-3: Institute of Techno-Economic Systems Analysis, D-52425 Jülich, Germany. E-mail: th.grube@fz-juelich.de*

[b]*PVcomB, Helmholtz Zentrum Berlin für Materialien und Energie GmbH, Schwarzschildstraße 3, D-12489 Berlin, Germany*

[c]*German Aerospace Center, Institute of Solar Research, Solar Chemical Engineering, Linder Hoehe, D-51147 Cologne, Germany*

[d]*RWTH Aachen University, Chair for Fuel Cells, Faculty of Mechanical Engineering, Kackertstraße 9, D-52072 Aachen, Germany*

† Electronic supplementary information (ESI) available. See DOI: 10.1039/d0se00896f

production *via* PEM and SOE-based hydrogen production units. These modules were then employed to determine the hydrogen yields at different locations from temperate to subtropical climates. Consequently, the economic performance of the concepts was examined in order to determine the levelized cost of hydrogen (LCOH) at each location.

The relevant literature on the topic of solar-based, electrolytic hydrogen production is divided into three groups of publications. The first considers experimental setups from laboratory-scale devices used as the basis for analyzing larger systems. Clarke *et al.*[5] coupled an electrolyzer to a solar PV system, proving the general concept of directly coupling PV and EL systems. In that study, a solar-to-hydrogen (STH) efficiency of 4.7% was experimentally achieved.[5] Privitera *et al.* demonstrated a vapor-fed alkaline anion exchange membrane (AEM) electrolysis system that achieved an STH efficiency of 15%.[6] Meanwhile, Muhammad-Bashir *et al.* realized STH efficiencies of up to 6.18% in a directly-coupled PV electrolysis system incorporating a V-shaped concentrator for enhanced sunlight collection.[7]

The second group of publications reports on theoretical research that was carried out in order to determine options and potential of solar hydrogen production. Turner *et al.* presented an overview of hydrogen production alternatives from renewable energy sources.[8] Jacobsson *et al.* discussed the difference in photoelectrochemical cells and PV-electrolysis systems and proposed a gradual nomenclature for these technologies to structure the research field of solar hydrogen generation.[9] Several other studies review recent research activities and assessment approaches related to the potential of renewable and solar radiation-based hydrogen production, respectively, on a theoretical scale, without going into details of the physical and chemical modelling of the subsystems.[10–13]

The modelling approaches found in the third group of publications aim to determine the potential of solar hydrogen production, analyzing distinct setups and system combinations, such as PV-PEM systems or photo-electrolysis (PEC) devices. On the one hand, these models can be further divided into bottom-up modelling approaches that were used to model the processes within the subsystems, allowing for the analysis of the dynamics performance of such systems. Sayedin *et al.*[14] employ a modeling approach for optimizing hydrogen generation by means of varying the size and operating conditions of a directly coupled PV-electrolyzer system[15] and also consider different irradiances[14] and locations worldwide.[16] García-Valverde *et al.* consider optimization procedures related to the direct coupling[17] and use of controlled DC–DC converters for PV-PEM systems.[18] The use of a V-trough-based PV generator is the focus of Su *et al.*,[19] who analyze the direct coupling of such a device with an electrolyzer. On the other hand, top-down models that determine hydrogen production with constant efficiencies for the subsystems also exist. In this respect, there is a literature focus on photocatalytic devices, which are analyzed in comparison to DC–DC coupled PV and PEM systems,[20] as well as on techno-economic analyses with costs ranging from 1.6–10.4 US$ per kg of hydrogen[21] or cost spans of 5.5–12 (ref. 22) and 1.5–4.0 US$ per kg.[23] Moreover, the life cycle analysis (LCA) of PV-electrolysis systems has been considered by Dumortier *et al.*[24] However, these analyses, including their theoretical upscaling, focus on a technology path at comparatively low technology readiness level (TRL), and are beyond the time horizon of our study. With a focus on large-scale electrolytic hydrogen production for different purposes, several studies provide cost estimates that are relevant in the context of our analysis. Fasihi *et al.*,[25] for instance, consider the large-scale production of liquid fuels from electrolytic hydrogen production based on electricity from a hybrid PV and wind power system. In the reference scenario, the levelized cost of hydrogen was estimated at 32.54 € per MW per h or 1.08 € per kg. Teichmann *et al.*[26] analyze different concepts for delivering electricity or hydrogen from regions with large renewable energy potential. For the case of PV-based, electrolytic hydrogen production in Northern Africa, the levelized cost of hydrogen was estimated to be 3.08 € per kg. Heuser *et al.*[27] consider a worldwide hydrogen provision scheme that rests upon potential global centers of wind or PV-based renewable power generation. Relating to the PV pathway, region-specific cost results range from 3.55–4.60 € per kg. Another cost estimate for STH concepts comes from Touili *et al.*,[28] who consider a PV-PEM system, presumably coupled without DC–DC converters. The analysis was carried out for 52 locations in Morocco, resulting in hydrogen costs ranging from 4.99–5.88 $ per kg.

Studies of the comparative analysis of STH concepts that include power generation by PV and CSP technologies are scarce in the literature. The work of Boudries[29] focuses on a hybrid solar-gas concept with CSP and PV for locations in Algeria and compares his results with information on PV-based concepts. The resulting hydrogen costs are in the range of 6–7 $ per kg. A study by Wang *et al.*[30] compares solar-driven thermochemical cycles with photo-electrochemical processes and PV-electrolysis concepts. However, no techno-economic analysis was performed in this analysis.

Going beyond published research, the specific objective of this study is to more consistently analyze and evaluate the techno-economic potential of candidate solar radiation-based, electrolytic hydrogen production pathways. This is accomplished through a consistent modeling approach that integrates the techno-economic analysis of four utility-scale STH concepts, including CSP and PV-based power generation, which are characterized by a high TRL and, thus, are expected to be available for large projects in the medium term. Moreover, the developed model is capable of using location-specific weather data that are most relevant to the techno-economic performance of the concepts analyzed. The common basis of evaluation is the solar collection area (aperture) of 1 km^2, which was derived from a state-of-the-art plant layout for CSP-based power generation. The concepts are analyzed and evaluated with respect to their economic performance and level of maturity. This is achieved by describing the fundamental pathway principles and discussing the subsystem's technology readiness levels (TRLs) at first and, secondly, modeling integrated solar hydrogen production systems with consideration to relevant physical and chemical parameters as well, as the systems' operational performance in a bottom-up approach.

After introducing that pathway principles and describing the technology readiness level in the next subsections, Section 2 introduces the relevant details on the concepts and applied methods of analyzing performance and cost. Section 3 presents the results of the analysis and their discussion, followed by the conclusion in Section 4.

1.1 Pathway principles

Fig. 1 displays relevant electrolytic solar-to-hydrogen pathway concepts according to the literature. These concepts are distinguished by power generation and electrolyzer technology and the degree of subsystem integration. The solar-to-hydrogen pathway alternatives analyzed in this study are two PV-PEM and two CSP-EL alternatives, highlighted in blue in Fig. 1. With respect to the conclusions drawn in our previous publication,[4] PV-PEM III and PV-PEM IV are only discussed against the backdrop of their general function and technology readiness level.

The CSP-EL pathways considered here uses different electrolyzer technologies. While in the CSP-SOE case, the electric power output of the CSP is delivered to a solid oxide electrolyzer, the CSP-PEM concept considers a polymer electrolyte membrane electrolyzer. Utility-scale CSP plants are typically realized as either a solar tower or a parabolic trough. In this work, a solar tower is considered and will be outlined in the following. Fig. 2 shows the related system configuration. The electric power generator is comprised of the subsystems' solar tower power block, the power cycle, power electronics and the electrolyzer system. Incoming solar radiation is reflected by the heliostat field to the receiver at the top of the solar tower. The receiver heats a thermal fluid by means of a heat exchanger. Surplus heat is stored in salt-based thermal storage and is used to bridge periods of low irradiation in the daytime or during the night, while sustaining a constant supply of heat to the thermal fluid. A second heat exchanger connects the thermal fluid cycle with the steam cycle for power generation. The CSP plant is then coupled to the electrolyzer *via* an AC/DC converter. As is mentioned above, the electrolyzer system used in our study is

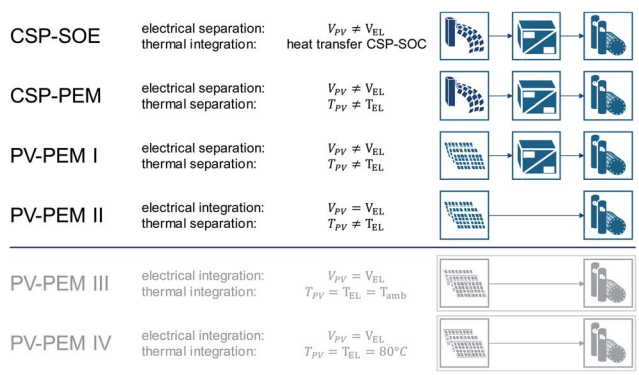

Fig. 1 Overview of electrolytic solar-to-hydrogen pathways with different concepts of subsystem integration; the top four pathways are focused by this study. CSP: concentrated solar power generator; EL: electrolysis; PEM: polymer electrolyte membrane; PV: photovoltaic generator; SOE: solid oxide electrolysis cell.

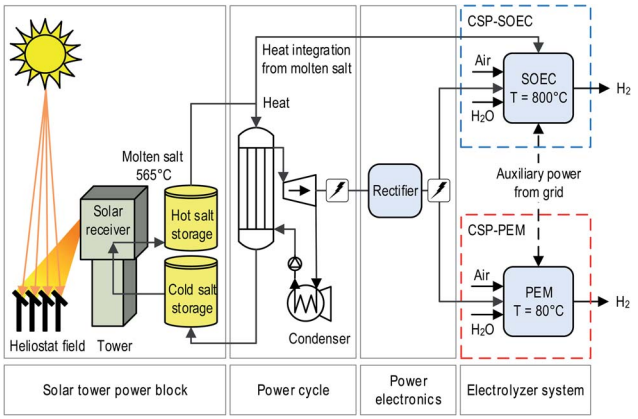

Fig. 2 Functional description of CSP-EL pathways. Adapted figure based on Roeb *et al.*[31]

based on either SOE or PEM technology. The SOE system additionally avails the opportunity of heat integration from the CSP plant. The hot product gases from the SOE process are used within the heat recovery system to pre-heat the steam close to the operating temperature of about 800 °C, before it is fed to the electrolyzer.

The PV-based pathways analyzed in this study are based on PEM electrolysis and are distinguished by the type of electrical integration, as can be seen in Fig. 3. The PV-PEM I concept operates with the PV and PEM subsystems being spatially- and thermally-separated and connected with a DC/DC converter. The converter adjusts the electrical output of the PV module to fit the operational characteristics of the electrolyzer. An advantage of the converter is that there are no coupling losses apart from the converter efficiency, which depends on the load level. Furthermore, the individual operating points of the PV and PEM subsystems do not have to be matched during the design phase. For the PV-PEM II concept, the PV and PEM subsystems are still spatially- and thermally-separated, but without the power converter.

PV-PEM III and photo-electrolysis, which are not considered in our simulations, show an even further integration level of the PV and PEM components. PV-PEM III omits the use of power

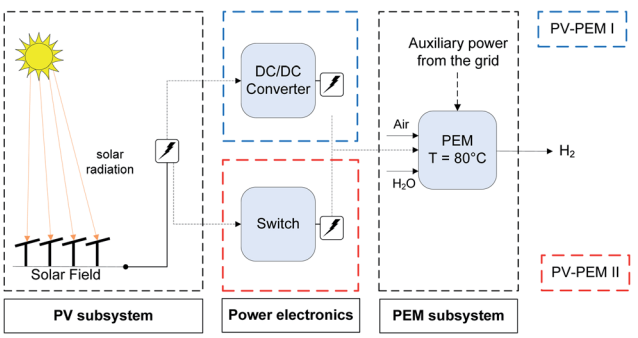

Fig. 3 Functional description of the PV-PEM pathways PV-PEM I and PV-PEM II considered in this study. Adapted figure based on Roeb *et al.*[31]

electronics, similar to PV-PEM II, and also brings PV and PEM subsystems together spatially. This causes an additional thermal coupling of the subsystems. Photo-electrolysis integrates the principles of photovoltaic power generation and electrolytic hydrogen production into a fully integrated single device. The semiconductor is here directly connected to the catalyst–electrolyte interface, where the hydrogen is generated.

1.2 Technology readiness level (TRL)

The solar-to-hydrogen pathways employ diverse technologies with different degrees of maturity, efficiencies and potentials. These divergent criteria are estimated based on information from the literature related to PV, EL and CSP. Based on standard TRL definitions according to Mankins (1995)[32] and EU (2014),[33] these findings are summarized into a TRL estimate for all subsystems under consideration. The relevant information collected in the literature can be found in the ESI, Section 5.1.†

Table 1 summarizes the TRL estimates for the different subsystems. PEM and – despite a lower TRL of 5 – SOE technology are of particular interest in the context of this study, as PEM is expected to be the dominant technology for sector coupling in the future and SOE technology can be beneficially applied in CSP systems due to its high efficiency potential through thermal system integration. These two technologies are therefore considered in this study.

The TRLs of the subsystems are linked to derive the TRL estimates related to the individual solar-to-hydrogen concept alternatives considered in this study. On the one hand, none of the described pathways was demonstrated on a commercial or larger laboratory scale. On the other, all of the pathways employ technologies with elevated and high maturity and TRLs of between five and nine. Following this fact, the determination of the TRLs is based on evaluating the prospects of realizing the respective STH pathway on a larger scale with consideration to the availability of the individual subsystems. Table 2 lists the TRL estimates of the different solar-to-hydrogen concepts. In the following, our TRL-related findings and the application potentials of the individual pathways will be briefly discussed.

The highest integrated system TRL is attributed to the concepts of PV-PEM with or without employment of power electronics (PV-PEM I and PV-PEM II) and CSP-PEM, as they incorporate subsystems with the highest individual TRL. Furthermore, the coupling of power generation and electrolysis *via* power converters does not impose any additional constraints that must be considered. Every subsystem can work independently and has been linked to other technologies in the past.[34] Thus, the theoretical setup could be easily realized, justifying the high TRL of eight for both pathways. The pathway PV-PEM III, directly coupling power generation and hydrogen production, is rated with a lower TRL of seven due to additional operational restrictions. The directly coupled and integrated pathway PV-PEM IV has only been realized on a laboratory scale, with, to our knowledge, no industrial scale in sight so far. Furthermore, the scaling of such systems would require the development of new technical components and seals. This is different to the pathways discussed above, which incorporate commercially available components coupled in new system layouts. Thus, the directly-coupled and locally-integrated PV-PEM IV pathway is rated with a TRL of five. All other pathways work with SOE electrolysis, which justifies the TRL rating of five for these.

For the subsequent analysis, we select CSP-SOE and CSP-PEM, as well as PV-PEM I and PV-PEM-II. Apart from SOE technology, which we chose for the reasons stated above, all technologies addressed are assumed to be ready for utility-scale solar-to-hydrogen projects because these are proven on the large megawatt scale. NREL provides a list of worldwide CSP projects that indicates that, at present, five power plants are operational with an individual capacity of more than 100 MW. The largest plant, which is located in California, has a net capacity of 377 MW.[35] Based on information in an IEA report, PV power plants are operational with capacities of more than 500 MW.[36] On a somewhat smaller scale, PEM technology is projected with 10 MW as part of the REFHYNE project and 20 MW at a hydrogen production facility of Air Liquide in Canada.[37] Both electrolyzers are expected to be operational in early 2021. Moreover, several projects on the 100 MW scale are under development.[38] Based on this information and with the exception of SOE technology, we anticipate no major hurdles regarding the feasibility of large-scale solar-to-hydrogen projects beginning in 2025.

Table 1 Technology readiness level (TRL) estimates of the solar-to-hydrogen subsystems based on our literature survey. The underlying information can be found in the ESI, Section 5.1[a]

Component technology	TRL
Photovoltaic (PV) power generation (SHJ)	9
Polymer electrolyte membrane (PEM) electrolysis	8
Solid oxide electrolysis (SOE)	5
Concentrated solar power generation (CSP)	9
Power electronics (PE)	9

[a] SHJ: silicon heterojunction technology.

Table 2 TRL estimates for solar-to-hydrogen pathways. Concept description – see Section 1.1

Pathway	TRL
PV-PEM I (PV-PEM + power electronics)	8
PV-PEM II (PV-PEM directly coupled)	8
PV-PEM III	7
PV-PEM IV	5
PV-SOE + power electronics	5
(PV-SOE direct)	5
CSP-PEM	8
CSP-SOE	5

2 Methods and assumptions

This section provides more details on the concepts considered in this study and presents the relevant model parameters and constraints, as well as the technical modeling approaches. The individual models of the subsystems are then outlined, before the interaction of the subsystems within the overall system of a solar-to-hydrogen concept is discussed.

2.1 Overall definitions and parameters

The calculation of the hydrogen production quantities *via* the selected pathways was conducted for specific locations based on hourly resolved time series of solar irradiation and ambient temperature. The locations chosen for the calculations were Oldenburg and Freiburg in Germany, Almeria in the south of Spain and Daggett in the Mojave Desert of the southwestern United States. Oldenburg and Freiburg are contrasting locations in Germany that resemble locations with a very low (Oldenburg) and elevated (Freiburg) exposure to solar irradiation over the year. Almeria is chosen to represent a Europe-wide and Daggett a world-wide maximum of solar irradiation. For both of the PV-PEM cases, all four locations are considered in this study. The analysis of the two CSP-EL cases is carried out on the basis of data from Almeria and Daggett only. Due to low direct irradiance, CSP plants are not considered to be commercially-feasible in Germany.

We chose the aperture area as the basis for comparing the pathway alternatives. As the design of the CSP led to aperture areas of 0.91 and 1.12 km^2 for Daggett and Almeria, respectively, we assumed 1.0 km^2 for the PV-based concepts.

With regard to the location-specific analysis, the two input parameters to the simulations are global horizontal irradiation (GHI) and ambient temperature. The GHI is derived from hourly values of the direct normal irradiation (DNI) and the diffuse horizontal irradiation (DHI) depending on the tracking process of the solar panels and CSP collectors. The CSP system employs two-axis tracking, which is inherent to this technology, while the PV system is modeled without tracking. The PV modules are oriented southward to the sun, as all observed locations are in the northern hemisphere. The tilt angle of the module's surface is equivalent to the latitude of the location to collect the maximum solar input. We used Typical Meteorological Year data from JRC's Typical Meteorological Data access service.[39]

Considering the concept alternatives selected in this study, the subsystems to be analyzed by means of simulation modeling are the photovoltaic module, the concentrated solar power generators, the electrolyzers and the power electronic devices. The technical models are complemented by an economic analysis of the subsystem cost in order to determine the levelized cost of hydrogen for each solar hydrogen production pathway. The cost data is estimated for the reference year 2025 and correlated to the short- to mid-term performance of greenhouse gas reduction technologies.

2.2 Subsystem models

The subsystems of the hydrogen production pathways considered in this study are the photovoltaic module, electrolysis system and power electronics. Subsystem models related to the PV-based concepts examined in this study are similar to those outlined in Reuβ *et al.* (2019).[4] The description is therefore short and contains only the most relevant approaches and parameters. For further information, please refer to Reuβ *et al.*,[4] where the CSP and SOE subsystems are presented in more detail.

2.2.1 Photovoltaic module. The PV model used in this study is the same as that in Reuβ *et al.* (2019).[4] The module data relate to the Panasonic VBHN330SA15 and have been derived from the SAM database.[40] The technical parameters of the module are listed in Table 3.

Also, in accordance with Reuβ *et al.*,[4] the *U–I* characteristics are modeled using the equivalent circuit, according to Tamrakar and Sawle,[41] that is displayed in Fig. 4.

The calculation uses a set of equations in accordance with De Soto *et al.* that require five parameters to outline the equivalent circuit[42] described by equation eqn (1):

$$I = I_{ph} - I_0\left[e^{\frac{U+IR_s}{a}} - 1\right] - \frac{U + IR_s}{R_p} \quad (1)$$

R_s: series resistance; R_p: shunt resistance; I_{ph}: light current; I_0: diode reverse saturation current; a: modified ideality factor, where parameter a is defined using eqn (2).

$$a = \frac{N_s n k T_c}{e} \quad (2)$$

These five parameters are typically provided by the manufacturer of the PV module in the respective datasheet. The parameters for the PV module of our choice are listed in Table 4, below.

2.2.2 CSP system. The concentrated solar power technology considered in this study is a molten salt solar tower, which is a point-focusing system that can heat salt to temperatures above 500 °C. This technology uses molten salt as both the heat transfer fluid and the thermal storage medium. If the storage is designed appropriately, it can allow for continuous operation and such technology is also currently commercially-available.[43] For this study, a thermal storage capacity of 16 full load hours was considered.

The parameters have been derived from the Greenius database[44] and the simulation was performed with the Greenius software, which was developed in order to provide performance calculation algorithms with hourly resolutions for concentrating solar power plants. The calculations are based on technology-specific parameters and the relevant location-specific meteorological data such as solar irradiation values and ambient conditions, as well as the wind direction and speed.

The most important power plant components and the associated parameters are subdivided in Greenius as follows:

(i) Collector and collector field (including geometric data, collector-specific values, field geometry, selection of heat transfer fluid)

Table 3 Module parameters[40]

Parameter	Value	Unit
P_{MPP}, power at MPP	330.6	W
U_{MPP}, voltage at MPP	58	V
I_{MPP}, current at MPP	5.7	A
U_{OC}, open circuit voltage	69.7	V
I_{SC}, short circuit current	6.1	A
U_{oc}, temperature coefficient	−0.170	V °C^{-1}
I_{sc}, temperature coefficient	0.002	A °C^{-1}

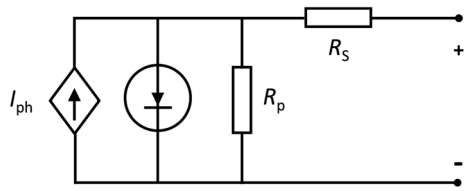

Fig. 4 Equivalent circuit of the one-diode-model.[41]

Table 4 Reference input parameters for the one-diode model approach, extracted from the SAM database[40] for the selected Panasonic PV Module VBHN330SJ47

Parameter		Value	Unit
$R_{s,ref}$	Series resistance	0.741	[ohm]
$R_{p,ref}$	Ohmic resistance	457.17	[ohm]
a_{ref}	Ideality factor	2.3402	[—]
$I_{ph,ref}$	Photo current	6.08	[A]
$I_{0,ref}$	Saturation current	6.88×10^{-13}	[A]
T_{NOCT}	Normal operating cell temperature	43.8	[°C]

(ii) Thermal storage (including the type of storage and storage capacity)

(iii) Power block (rated power)

The parameters of the overall CSP system are listed in Table 5.

2.2.3 Rectifier and power converter. Two types of power electronic devices were used for the modeling in this study, namely a rectifier and a DC/DC converter. The power converter was used to adjust the DC power output of the PV module to fit the DC power characteristics of the electrolyzer within the PV-PEM I concept. The rectifier transforms the alternating current from the CSP plant into direct current, which is then used as the input for the electrolysis. The efficiencies of both components are dependent on the actual load state and the correlations were derived from the SAM database.[45] We assume that the power electronics are not capable of operating above the design point for longer time periods. For this reason, the input power into the power electronics must be kept below or at the nominal power level across the entire operational range. This is achieved by curtailing the input power to the nominal power in the case of an energy excess of above 5%.

2.2.4 PEM and SOE electrolyzer. The modeling approach of the two electrolyzer types, SOE and PEM, are based upon the characteristic polarization curve, which depicts the dependency between the current density j and voltage U.

The operational behavior of the SOE is approximated with a linear equation, as the activation overpotentials decrease due to improved reaction kinetics at the operating temperature of 700–800 °C. The following reference points are used:[46]

$$j_0 = 0 \text{ A cm}^{-2};\ U_0 = 0.95 \text{ V} \quad (3)$$

$$j_1 = 0.75 \text{ A cm}^{-2};\ U_1 = 1.1 \text{ V} \quad (4)$$

The cell efficiency of the SOE is assumed to be constant across the entire operational range. This is due to two opposing

Table 5 Parameters for the CSP technology design

Site position and orientation	Almeria (Spain)	Daggett (USA)	Dimension
Latitude	36.83	34.85	°N
Longitude	−2.45	−116.8	°E
DNI	1918	2723	kW h m^{-2}
CSP technology			
Solar tower			
Heat transfer fluid	Molten salt		
Heliostat field			
Heliostat reflective area	121.3	121.3	m^2
Clean mirror reflectivity	0.94	0.94	
Total reflective area	1 118 626	910 440	m^2
Tower height	182.5	176.3	m
Receiver			
Receiver intercept power	500	500	MW
Receiver inlet temperature	292	292	°C
Receiver outlet temperature	565	565	°C
Receiver outlet power	433	440	MW
Efficiency of heat transfer fluid pump	98	98	%
Powerblock and storage			
Nominal electrical output	70.4	70.4	MW_{el}
Type of storage	Two-tank molten salt		
Thermal storage capacity	2600	2600	MW h

effects, which are both proportional to the load of the electrolysis system. On one side, the cell efficiency increases with decreasing partial load. On the other side, the heat demand increases proportionally with decreasing partial load, as the electrolyzer is not operated under thermo-neutral conditions. The constant cell efficiency at the thermo-neutral point of 113% exceeds 100% because the actual cell voltage is below the water-splitting potential of 1.23 V. Similar to the PEM case, the electrolyzer stack current I_{SOE} is calculated by multiplying the current density j by the active electrode area A_{SOE}. This area is determined within the design phase of each pathway and is optimized depending on the location-specific solar irradiation and power characteristics of the employed PV subsystem. The active electrode area also defines the installed capacity of the electrolysis system. The optimization considers the most cost-efficient relationship of the installed electrolysis to PV capacity.

For the PEM electrolyzer, the model for determining the U–j-curve is, as in Reuß *et al.* (2019),[4] based on Tjarks *et al.* (2018).[47] The respective equations are:

$$U_{cell} = 1.185 \text{ V} - \alpha(T) \times \ln\left(\frac{j}{j_0(T)}\right) + j \times (R_{ion}(T) + 0.025\ \Omega + 0.096\ \Omega) \quad (5)$$

$$\eta_{EL,cell} = \frac{H_u}{2 \times e \times N_A \times U_{cell}} \quad (6)$$

The PEM electrolyzer current I_{PEM} is the product of the current density j and the electrochemically-active area A_{PEM}.

In addition to the losses within the electrolysis cell, the auxiliary power of the balance-of-plant (BoP) components such as pumps and heaters must be considered. Within this model, the auxiliary power of the SOE and PEM electrolysis is assumed to be a fixed share of the electrolyzer systems' nominal power $P_{EL,nom}$ across the entire operational range. For the SOE and PEM electrolysis, this share is set to 2% and 5%, respectively. Furthermore, the auxiliary power demand has no influence on the system efficiency of the electrolysis system, as it is assumed to be covered by the connected power grid. The power that is drawn from the grid is also accounted for within the economic analysis. Faradaic losses are neglected in this analysis, as the electrolysis system is operated under atmospheric conditions. The operational limit is addressed by curtailment in the case of excess voltage above the nominal system voltage in order to avoid increased cell decay. The pathways, which incorporate power electronics, decrease the power supply to the electrolyzer to the maximum voltage input. For the PV-PEM II systems that do not contain a converter between the PV and EL subsystems, the power supply is cut to zero, when the input voltage exceeds the nominal voltage input by 5% or more.

2.3 Subsystem interaction and coupling

Depending on which hydrogen production pathway is considered, the interaction and coupling of the subsystems differ (*cf.* Section 1.1). This study considers four different STH pathways, each with an approximate solar collection area of *ca.* 1 km^2. The functional schemes of these pathways are displayed in Fig. 1.

Hydrogen production *via* a CSP plant connected to an electrolyzer is determined by considering two alternative electrolysis technologies. The pathway CSP-SOE uses the SOE-technology to generate hydrogen from electricity and heat. As the SOE electrolyzer operates at high temperatures of 700–800 °C, the possibility of heat integration from other processes exists. This model considers heat integration from the molten salt cycle of the CSP plant (see Fig. 2). The integrated heat is deployed for pre-heating and steam generation before the feed steam is introduced into the electrolyzer. The nominal size of the CSP plant is set to 70 MW_e, while the electrolyzer's capacity is equivalent to the CSP system's nominal power. In order to achieve this, the aperture area of the CSP plant in Almeria is set to *ca.* 1.12 km^2 and in Daggett to 0.91 km^2. The divergence is attributed to different solar irradiation levels between the locations. The pathway CSP-PEM couples the CSP-plant to a PEM electrolysis stack in which a rectifier is employed to convert the alternating current of the CSP plant into direct current. The efficiency of the rectifier is also dependent on the partial load, as depicted below, in Section 3.2.

The nominal power of the electrolysis system for the pathways PV-PEM I and PV-PEM II is subject to optimization because there is a trade-off to be made between investment costs and electrolysis efficiency. Related to this optimization, the ratio of electrolysis and PV power is varied within an interval of 0.5–1 of the nominal power for each location. The ratio that leads to minimal hydrogen production cost is used as the design point. For the PV-PEM I concept, it is assumed that the nominal power of the power electronics is equal to that of the electrolysis system. The result of the optimization method is shown in Section 3.2. The operating point for PV-PEM II is found by overlaying the *U*–*I*-curves of the subsystems. An electrolysis cell operates between 1.5–2 V, while the PV module has an output voltage of about 45 V. In order to approximate the operating points, the voltage of the electrolyzer is multiplied by the number of electrolysis cells, so that an optimal fit of operating points is accomplished. This adjustment is performed during the design phase. Whenever the operational conditions deviate from the nominal design point, the EL curve does not cross the PV curve close to the Maximum Power Point (MPP) of the PV Module. This results in losses, as there is only part of the maximum PV power output being harnessed. These coupling losses then lead to the definition of coupling efficiency:[48]

$$\eta_c = \frac{P_{OP}}{P_{MPP}} = \frac{J_{OP} \times U_{OP}}{J_{MPP} \times U_{MPP}} \quad (7)$$

The nominal power of the PV subsystem is related to the solar collection area of the CSP plant to approximate the solar input energy of both pathways. The aperture area is set to 1 km^2, which leads to a nominal power of 197.6 MW_e for the PV subsystem.

2.4 Economic analysis

This section outlines the necessary investments and operational costs (OPEX) of the PV, CSP and EL subsystems. These parameters are used to find the overall cost for all of the pathways under consideration. The economic analysis is conducted for the reference year 2025. Possible revenues from selling surplus electricity to the grid are not considered in this study.

Investment in the hydrogen production pathways is calculated as the product of specific investment [€ per kW_p] and the installed nominal power [kW_p], while the operational cost OPEX [€ per a] is determined from the operation and maintenance (O&M) cost, which are estimated using a given percentage of the investment cost:

$$\text{INVEST} = \text{specific investment cost} \times \text{installed nominal power} \quad (8)$$

$$\text{OPEX} = \text{O\&M} \times \text{INVEST} \quad (9)$$

Section 3.1 presents the total annual cost (TAC) [€ per a] as the sum of the annuity factor multiplied by the investment and operational costs (OPEX):

$$\text{TAC} = \text{ANN} \times \text{INVEST} + \text{OPEX} \quad (10)$$

The annuity factor ANN is determined with a fixed interest rate i of 8% and the depreciation period n:

$$\text{ANN} = \frac{(1+i)^n \times i}{(1+i)^n - 1} \quad (11)$$

The levelized cost of hydrogen LCOH is then determined from the TAC and annual hydrogen production by:

$$\mathrm{LCOH} = \frac{\mathrm{TAC}}{\text{annual hydrogen production}} \quad (12)$$

The various factors affecting the levelized cost of hydrogen (LCOH) are discussed in the Results section 3.5.

2.4.1 Photovoltaic systems. The costs of photovoltaic systems are dependent on the semi-conductor material used, the installed capacity, as well as the countries of production and installation. Furthermore, PV technology is subject to constant cost reductions due to efficiency improvements and economies of scale. These factors must be considered when evaluating the cost of photovoltaic systems. This cost can be broken down into the PV module price, the cost of the balance-of-system (BoS) components and the inverter cost. According to the photovoltaics report from the ISE Fraunhofer, the module price constituted 47%, while the BoS and inverter cost accounted for 53% of the overall PV system investment cost in Germany for the year 2016.[49] The installed system price for utility-scale applications, including the inverter, is set to an average of 1.25 € per W_p.[49] The PV system prices for the United States differ from those in the German market and were estimated to an average of 2.2 € per W_p for large-scale applications in 2016 by a report by the Lawrence Berkeley National Laboratory.[50] Another study from the U.S. Department of Energy estimated PV system prices in the range of around 2 € per W_p, with local deviations within the country.[51] The prices for PV systems in the United States are higher by comparison to German prices due to higher installation and BoS costs.[52] The investment costs for inverters are estimated to be 100 € per kW_p for the year 2025, according to the IRENA report.[53] The current market prices for SHJ modules, which are modeled in this study, are higher than for silicon or thin film modules. However, as silicon heterojunction is a relatively new technology in the PV market, near-term cost reductions for such modules are expected to be higher than for other PV technologies, as the effects of efficiency improvements and economies of scale are more significant. This justifies the assumption that SHJ module prices will approach those of silicon and thin film technologies against the reference year of 2025. In accordance with this assumption, the cost projection for this reference year on the basis of the average module prices, indicated above, will be adopted for the SHJ module price for the reference year 2025. The specific investment cost of the PV system in the year 2025 is set to 800 € per kWp and the O&M factor to 2% of the CAPEX, according to the IRENA report from 2016.[53] The depreciation period for the PV system was assumed to last 25 years.

2.4.2 Concentrated solar power generation. The commercial CSP technology can be subdivided into two dominant types of power generation, namely the parabolic trough collector (PTC) technology and solar towers (ST). Although PTC systems account for 85% of the installed CSP capacity worldwide, ST can achieve higher efficiencies, especially within the steam cycle due to higher process temperatures. In addition, the higher process temperatures favor the combination of ST technology with solid oxide electrolysis. Therefore, this study focuses on the ST technology. The economic data for investment and operational costs are derived from the IRENA report from 2015.[53] The main contributors to the investment cost of an ST are the owner's cost, the indirect EPC (engineering, procurement and construction) cost, thermal storage, the power block, the tower, the receiver and the solar field. In 2015, the investment cost for ST plants was 5700 € per kW installed electric capacity for a typical plant with a heat storage capacity of up to 9 h. Due to reductions in the EPC cost, investment costs are projected to decrease to 3600 € per kW_e installed electric capacity towards the year 2025.[54] This value is used in this study. For a more detailed economic assessment, the investment cost is determined with the component cost data derived from the DLR report.[54] The investments costs of the solar tower system can be divided into three major components: that of the heliostat field, the tower and the receiver, which are 103 € per m^2, 72 000 € per m and 100 € per kW per h_{th}, respectively. The specific thermal storage cost is 22 € per kW per h, while the power block cost amounts to 1100 € per kW. The O&M factor is estimated to have been about 4% of the CAPEX in 2015. The projection for the year 2025 is assumed with a reduced O&M factor of 3% of CAPEX owing to improvements in the durability and consumption of the system over time. The lifetime of an ST plant is assumed to be 25 years.

2.4.3 Electrolysis. The current market for electrolysis systems is dominated by the highly commercialized alkaline electrolysis technology. With PEM and SOE electrolysis under further development, these technologies will steadily push into the market over the coming years to challenge the dominance of alkaline electrolysis on the basis of their beneficial operational characteristics.[55]

The investment cost of PEM electrolysis systems is highly sensitive to the installed capacity. Furthermore, the reference year has an impact on the investment cost, as the PEM technology is expected to undergo rapid price reductions due to further optimization and economies of scale. Smolinka *et al.* determined a specific investment cost of 1200 € per kW_{input} for mid-term development and large-scale application. The O&M factor was set to 4% of the CAPEX.[55] Bertuccioli *et al.* conducted a study for the Fuel Cells and Hydrogen Joint Undertaking (FCH JU) that included a cost projection for PEM electrolysis. The investment cost for PEM electrolysis over the installed capacity in 2015 was indicated with 1570 € per kW_{input} as an average over the installed capacity. The cost projection revealed an expected cost decrease to 1000 € per kW_{input} for the year 2020 and 870 € per kW_{input} for the year 2025 with an operational cost of 2–5% of CAPEX.[56] Saba *et al.* reviewed the literature on electrolysis costs for the last 30 years and determined a specific investment cost of 516 € per kW_{input} for alkaline electrolysis for the year 2014, assuming an atmospheric system and installed capacity of 2.5 MW.[57] The cost gap to pressurized systems was indicated at 20%, constituting a major influence. This emphasizes the strong dependency of the investment cost on the installed capacity of the system. Large-scale applications show price reductions because auxiliary devices do not scale with the installed capacity. Mergel *et al.* calculated an investment cost of

585 € per kW_{input} for the year 2013 for a large-scale PEM electrolysis system.[58] The study PlanDelyKad determined an investment cost of 363 € per $kW_{HHV\text{-}output}$ for a 100 MW PEM electrolyzer for the reference year 2014. The operational cost in this case was assumed to be 2% of the CAPEX.[59] These studies share a strong dependency of the investment cost on the reference year, the nominal capacity of the system and whether or not the electrolyzer is operated under pressure. Furthermore, the assumed system efficiency determines the difference between the investment cost referenced to the input and those referenced to the output power. In this study, an investment cost of 600 € per kW_{input} is assumed for atmospheric operation in the year 2025. The O&M factor is set to 2% of the CAPEX. The depreciation period n is 10 years, which is shorter than that of the power generation technologies because of the lower TRL of electrolysis concepts assumed here. However, within the cost sensitivity analysis in Section 3.5, we have also considered a case with a 25 year depreciation time.

The SOE technology is still at the laboratory stage, with no commercial application as yet. The cost estimations and projections vary across a broad range due to the early developmental stage of the technology. Schmidt *et al.*[60] conducted a survey of experts from industrial and research institutions to determine current and future costs for electrolysis technologies. They found that the expected investment cost of SOE applications would be in the range of 3000–5000 € per kW_{input} for the year 2020. The projection for the year 2030 settled the investment cost at between 1050–4250 € per kW_{input}.[60] These results stress the fact that cost predictions for SOE applications are dependent on the qualified estimations of experts, rather than actual market research. Based on the cost projections given above, the specific investment cost used in our study is defined with 2000 € per kW_{input} for an installed capacity of 70 MW and the reference year 2025. The O&M factor relative to CAPEX and the depreciation period are set to 2% and 10 years, respectively, both in analogy to the PEM electrolysis system. For the lower depreciation period, we applied the same reasoning as for PEM electrolysis. The electricity demand of auxiliary components, such as pumps, heaters, dryers and compressors is drawn from the grid. Based on recent and current values and assuming a continuous trend of reduced electricity cost for industry over time, with the electricity price for economic consideration set to 0.06 € per kW per h.[61]

2.4.4 Power electronics. As mentioned above, rectifiers for the coupling of the CSP plant to the electrolysis system and DC/DC converters for the junction between the PV and the EL system are considered. According to the IRENA Report, inverters for PV systems are assumed to have an investment cost of 100 $ per kW in the year 2025.[53] The same investment cost is employed for the rectifier in this model, as these devices incorporate similar technical components. For DC/DC converters, an investment cost of 100 € per kW, an O&M factor of 2% and a depreciation period of 25 years are assumed.

2.5 Cost summary

The overall capital cost of the PV-PEM and CSP-EL pathways is determined by the sum of the subsystem's capital cost, calculated here as the annuities for each pathway. Table 6 summarizes the specific investment, operational cost rate and depreciation period per STH pathway and location considered. The shorter depreciation periods used for the PEM and SOE subsystems are discussed in Section 2.4.

3 Results and discussion

This section discusses the results of the hydrogen production predictions of all the pathways using the model-based calculations. After introducing location-specific irradiance levels, the results from optimizing the PV-based concepts of PV-PEM I and PV-PEM II for the four locations with respect to the nominal power ratio of electrolysis and PV module (see Section 2.3) are presented. Based on this optimization, the nominal power and aperture area are presented, followed by the overall hydrogen production volume. Subsequently, the levelized cost of hydrogen by production concept and location are presented. A sensitivity analysis regarding the selected techno-economic parameters completes the analysis.

3.1 Location-specific irradiance levels

Fig. 5 depicts the irradiance profile for Oldenburg in Germany and Daggett in the USA to exemplarily visualize the locations with the lowest and highest irradiance distribution, respectively, over the year. As can be seen for both locations, irradiation is generally higher and shows longer duration during summer days. The irradiance profiles for the other locations have similar seasonal courses over the year, but at different total irradiance levels. The respective profile representations can be found in Section 5.2 of the ESI.†

The hourly resolved weather data irradiance and ambient temperature translate into yearly averages, which are shown in Table 7. As could be expected, the highest average irradiance was found for Daggett, followed by Almeria, Freiburg and Oldenburg. This trend is similar for the average ambient temperature with the exception of Oldenburg, which has a slightly higher value compared to Freiburg.

3.2 Design parameters

With regard to the optimization of the PV-PEM concepts, Fig. 6 depicts the hydrogen production cost for all four locations with consideration to an increasing nominal capacity ratio of EL and PV in the range of 0–100%. In general, the STH efficiency increases at higher EL- to PV-power capacity ratio because of higher electrolysis cell efficiencies, which are caused by a larger active electrolyzer area and, therefore, lower operational voltages. However, a higher active area translates into higher investment costs for the electrolyzer system. The optimum EL-PV capacity ratio is found at diverging values due to diverging irradiation characteristics per location. For Oldenburg and Freiburg, the optimum ratio is 0.5 for the PV-PEM I concept, while the optimum ratio for all of the other cases is 0.7. For the cases under consideration, it can be concluded that in locations with higher irradiations, a higher EL-PV ratio is beneficial, as more electric power is supplied to the electrolysis system.

Table 6 Economic parameters for each technology used in this study for the base year of 2025

Subsystem	Specific investment cost [€ per kW_p]	O&M [% of investment cost]	Depreciation period [years]
PV	800	2	25
CSP	3600	3	25
PEM	600	2	10
SOE	2000	2	10
Power electronics	100	2	25

Nevertheless, the locations of higher irradiance lead to the lowest optimized hydrogen production costs because of the higher hydrogen yield. It must be noted, that surplus electricity from solar generation that could not be consumed by the electrolyzer has not been considered in this analysis. If fed into the grid, additional revenues could improve the overall plant economics.

Following this optimization, the electrolyzer system and power electronics have a nominal power of *ca.* 138 MW for Almeria and Daggett and 119 MW for Oldenburg and Freiburg. Considering the definitions related to the CSP-based concepts, Table 8 lists the nominal capacity values of the subsystems, as well as the aperture areas of all pathways.

In accordance with the different subsystems' nominal capacities, the annuity results differ by location. Related to the PV-PEM I and PV-PEM II concepts, the electrolyzer capacity differs by location and is larger in Almeria and Daggett because the irradiation at these locations is generally higher. According

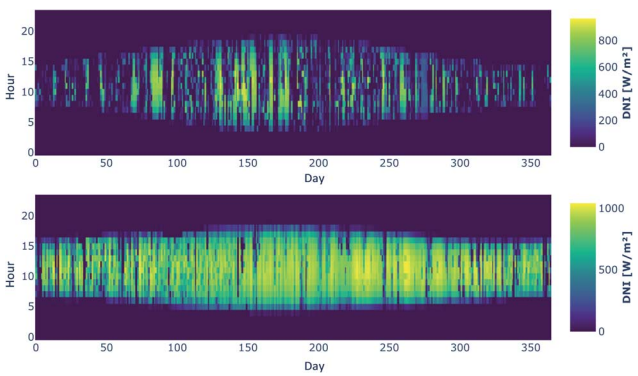

Fig. 5 Irradiance profile for Oldenburg/Germany (upper) and Daggett/USA (lower).

Table 7 Yearly averaged irradiances and ambient temperatures over one year

Location	Average irradiance [W m^{-2}]	Average ambient temperature [°C]
Oldenburg	259.7	11.0
Freiburg	289.4	9.7
Almeria	517.5	18.7
Daggett	525.9	19.7

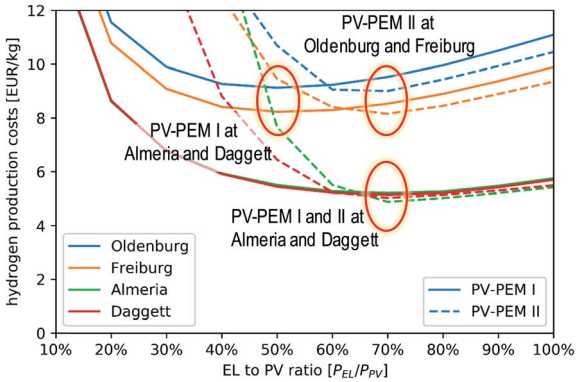

Fig. 6 Optimization of the nominal power ratio of PV and EL subsystems.

to the defined scope of this study, the annuity calculations for the CSP-EL concepts are carried out for Daggett and Almeria only (*cf.* Section 2.1). Fig. 7 displays site-specific investment and total annual cost (TAC) for all concepts under consideration. The related investment and TAC of the CSP-SOE pathway are highest because of the higher specific investment costs of CSP and SOE technology. Moreover, PV-PEM I requires somewhat higher investment than PV-PEM II, as the reduced electrolyzer investment, based on the design optimization, does not fully compensate for the power converter investment.

3.3 Hydrogen production quantity

This section presents and discusses overall hydrogen production at the locations of Oldenburg and Freiburg in Germany (PV-PEM only), as well as Almeria in Spain and Daggett in the USA (all concepts).

Fig. 8 depicts the monthly hydrogen production for Oldenburg and Daggett bearing the lowest and highest hydrogen yield, respectively, of all the locations considered. The related figures for Freiburg and Almeria can be found in Section 5.3 of the ESI.† The figures clearly show a seasonal dependency of the hydrogen production quantity, highlighting an increased hydrogen production level during the summer months, which is correlated with higher irradiation during that time, as is shown in Section 2.1.

The hydrogen production for the CSP-EL pathways is significantly higher than for the PV-PEM pathways. This is due to differences in the design phase. All of the pathways are designed for a solar collection area of *ca.* 1 km^2, resulting in a nominal electrical output of 70 MW_e for the CSP-EL pathways, 138 MW_e in Almeria and Daggett and 119 MW_e in Freiburg and Oldenburg for the PV-PEM I and II pathways, respectively. Although the nominal electrical output of the PV subsystems is higher, the average yearly power generation is below that of the CSP plants. This comes down to a difference in the definitions of the nominal operating points between the PV and CSP subsystems. The nominal operating point of the PV modules is equal to the maximum power point at an irradiation of 1000 W m^{-2}, while the nominal output of the CSP plants equals the average electrical output. In order to compare the pathways'

Table 8 Nominal subsystem power and aperture areas of all pathways

	PV/CSP [MW]	Electrolyzer [MW]		Aperture area [km^2]	
Pathways	All locations	Almeria/Daggett	Freiburg/Oldenburg	Daggett	Almeria
CSP-SOE	70.43	70		0.91	1.12
CSP-PEM	70.43	70		0.91	1.12
PV-PEM I	205.55	138.32	119.56	1.00	
PV-PEM II	205.55	138.32	119.56	1.00	

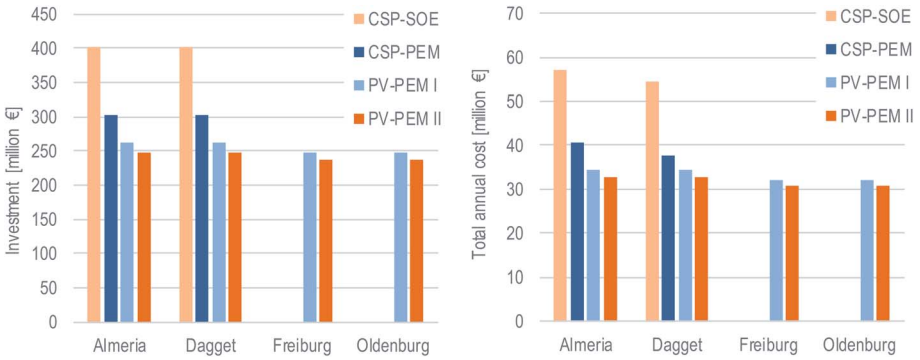

Fig. 7 Investment (left) and total annual cost (right) for all concepts considered [€ per a] for different locations.

competitiveness, the LCOH must be considered, as the higher total hydrogen output of the CSP-EL pathway goes in line with higher investment costs. The LCOH will be discussed in Section 3.4. The hydrogen production from the pathway CSP-SOE is significantly higher across the entire year than production *via* the CSP-PEM pathway. This is explained by a better electrolysis performance, as the CSP plant, power electronics and design points are equal for both pathways.

Related to the PV-PEM concepts, the hydrogen production of PV-PEM I is, consistently, somewhat lower compared to PV-PEM II for the location of Oldenburg. For Daggett, there is no clear tendency; only between May and September is the H_2 yield of PV-PEM I somewhat higher compared to PV-PEM II. The expected increase caused by better coupling efficiency is not evident. Accordingly, the average STH efficiency for PV-PEM I is lower than that for PV-PEM II, with 11.2% compared to 12.8%.

Fig. 9 gives an overview of total annual hydrogen production across all pathways and locations. Additionally, with the divergences between the hydrogen productions of the different pathways, the dependency on the location can be observed. From Oldenburg to Daggett, the total hydrogen production increases with average irradiation. The total STH efficiencies as the ratio of the hydrogen yield (based on the lower heating value) and irradiation G range from 11–13% for the PV-based concepts and 12–18% for the CSP-based ones. The highest values are found for CSP-SOE at Almeria with 16% and Daggett with 18%, which is consistent with the significantly higher hydrogen yields.

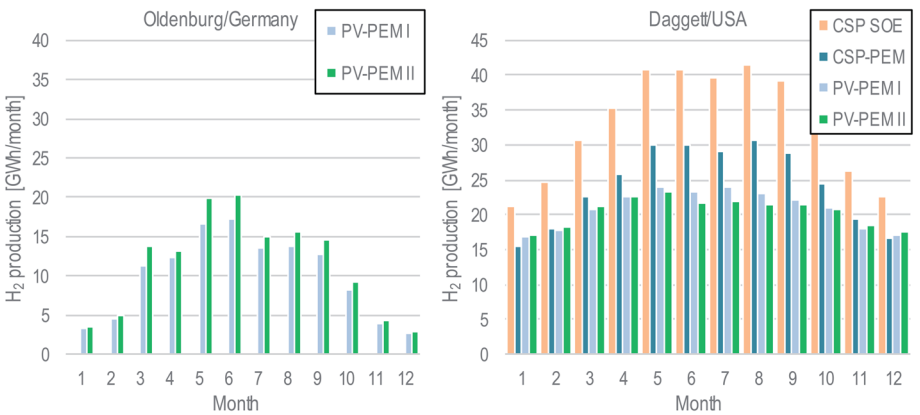

Fig. 8 Monthly hydrogen production for Oldenburg (left) and Daggett (right) in the base year 2007.

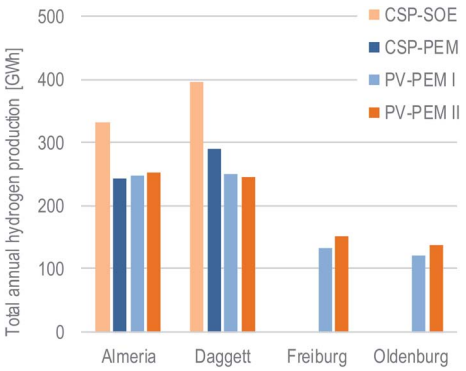

Fig. 9 Total annual hydrogen production for different pathways per location using meteorological data from 2007.

3.4 Levelized cost of hydrogen

The techno-economic analysis shows the levelized cost of hydrogen for all pathways at each location; see Fig. 10. The hydrogen generation cost for the locations of Oldenburg and Freiburg is nearly twice as high as the hydrogen cost in Almeria and Daggett. This reveals a direct correlation of the solar resource to the LCOH. The LCOH of the pathways PV-PEM I and PV-PEM II are nearly the same, with a very slight tendency towards lower LCOH for PV-PEM II. This shows that there is, on the one hand, no significant cost reduction achievable by coupling the subsystems PV and EL directly. Since, on the other hand, the hydrogen production volume is somewhat higher for PV-PEM II, the direct coupling has a slight advantage over coupling through a power converter, in the optimized system.

The comparison of the CSP-SOE and CSP-PEM pathways shows no cost advantage of one pathway over the other. As the hydrogen yield of the CSP-SOE concepts is significantly higher, this concept might be the better choice. Comparing the PV-PEM and CSP-EL concepts, PV-PEM shows little lower LCOH for Almeria and little higher LCOH for Daggett, the latter featuring the higher irradiance of the two locations. Cost differences are, however, small. The cost of all four concepts range between 14 and 17 ct per kW per h at the locations of Almeria and Daggett.

For the reference year 2020, the pathway-independent DOE targets for the LCOH are set with 6 $-ct per kW per h. This target is only valid for hydrogen production. Within our model-based analysis, this goal could not be achieved. The lowest cost levels are derived for the CSP-PEM and CSP-SOE concepts in Daggett, with 0.14 € per kW per h. The cost breakdown by concept and location shown in Fig. 11 reveals, as could be expected, that the major cost drivers are power generation *via* PV (PV-PEM concepts) and CSP (CSP concepts), the latter having an even greater cost share of the total costs. Because of this, the effect of varied investment costs might reveal cost reduction potentials for the concepts analyzed in this study. The costs and thus cost share of the solar conversion technology, whether PV or CSP, increases for areas with lower irradiance.

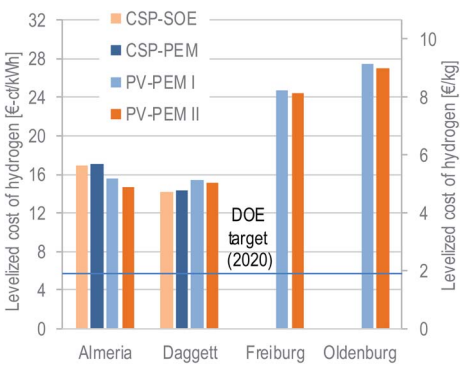

Fig. 10 Levelized cost of hydrogen using costs projected for 2025 with meteorological data from 2007.

3.5 Cost sensitivity

As was shown above, the hydrogen cost of STH concepts are driven by the component investment. The following sensitivity analysis varies the specific investments given in Table 6 by 20% in both directions, *i.e.*, decrease and increase. Moreover, we have chosen to vary the WACC (weighted average cost of capital) which is, in reality, subject to variation, *e.g.*, by region and might, therefore, have a significant impact on the annual cost and total hydrogen production cost. Finally, we assume an increased depreciation period of 25 years for the electrolyzers, bringing this parameter in line with the assumptions for power generation and power conversion. The explanations below are given on the basis of the results for selected locations, namely Oldenburg (lowest irradiation levels) and Daggett (highest irradiation levels). The full set of graphic representations of our sensitivity analysis is shown in Section 5.4 of the ESI.†

The results of our sensitivity analysis relating to the location of Oldenburg are displayed in Fig. 12. A decreased PV investment and WACC would reduce the hydrogen cost by 10% and 8%, respectively. Also, for these concepts an increased depreciation period of 25 years would be highly beneficial with a 12% (PV-PEM I) and 13% (PV-PEM-II) cost decrease, respectively.

Fig. 13 shows the results of the respective sensitivity analysis related to the two CSP-EL concepts at the location of Daggett. The impact of the selected parameters on the LCOH ranges between 8% and 15%. For the CSP-SOE concept, the lifetime extension has the greatest impact with 14%, followed by the reduction of CSP investment with 11%. The latter also has the most significant impact on the CSP-PEM concept with 15%. The second is the WACC which, if reduced, would decrease the cost of hydrogen by 9%. Lifetime expansion is also the most significant for PV-PEM II.

Our results also show that of all the pathway power generation technologies, CSP and PV have a higher impact on the LCOH than the electrolysis technologies.

3.6 Cost reduction potential

In the final step of our cost assessment, we combine the individual assumptions aimed at reducing costs to identify an overall cost reduction potential for the concepts considered in this study.

The results of combining the cost reduction factors considered are shown for the CSP-SOE concept in Fig. 14. It can be

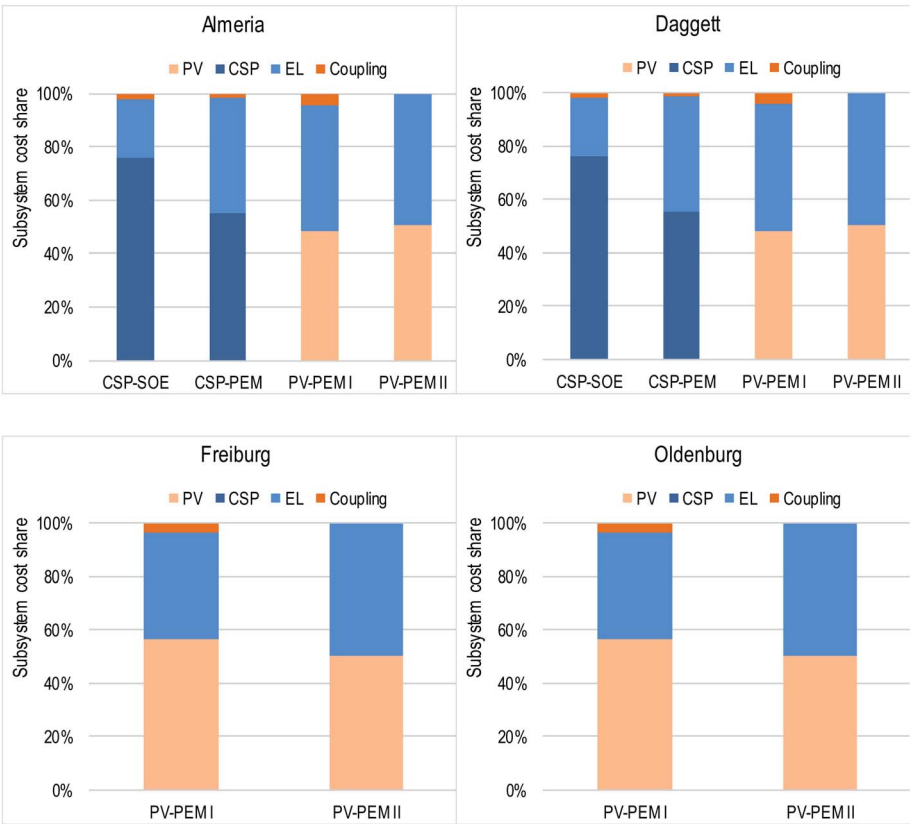

Fig. 11 Break-down of contributions to the hydrogen production cost by subsystem cost.

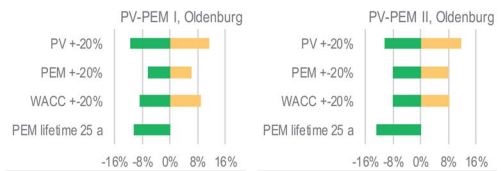

Fig. 12 Cost sensitivities of the PV-PEM I and PV-PEM II concepts for the example of Oldenburg/Germany.

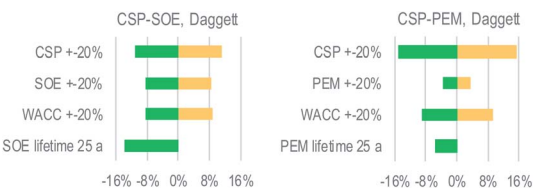

Fig. 13 Cost sensitivities of the CSP-SOE and CSP-PEM concepts for the example of Daggett/USA.

seen that the hydrogen production cost could be reduced to a level of 9–11 €-ct per kW per h (3.00–3.67 € per kg_{H_2}) for Almeria and Daggett if it was possible to reduce the investment costs of the CSP and SOE by 20%, extend the depreciation period of SOE to 25 years and if a reduced WACC of 6.4% would be applicable. The respective costs for the CSP-PEM (see Section 5.5 in the ESI†) would be slightly elevated to 10–12 €-ct per kW per h (3.33–4.00 € per kg_{H_2}).

Related to the PV-PEM I concept, our analysis reveals similar cost levels of 10 €-ct per kW per h (3.33 € per kg_{H_2}) under our most optimistic assumptions for Almeria and Daggett. Due to significantly lower irradiation levels in Oldenburg and Freiburg, the cost level is higher, at 16–18 €-ct per kW per h (5.33–6.00 € per kg_{H_2}) (Fig. 15).

Comparing our results with the values from the literature allows us to conclude that our estimates are typically higher than those reported the literature. Besides the time horizon of the individual studies, several parameters that have been differently assumed have a major impact on the cost estimates. In particular, the electricity cost, electrolyzer investment and annual full-load hours, as well as the interest rate and depreciation time, must be named in this context. The study by Fasihi *et al.*[25] assumes a specific electrolyzer cost of 319 € per kW_e for an alkaline electrolyzer and a depreciation time of 30 years, which strongly contributes to the decreased hydrogen cost level of 1.08 € per kg. Moreover, the study assumes a hybrid wind and PV power plant, allowing for high annual full-load hours of more than 6800. This is significantly higher than the full-load hours in our analysis, which are 5700 in the best case scenario. The results of the work by Teichmann *et al.*,[26] which also relates to PV-electrolysis pathways, show that, based on more moderate assumptions regarding electrolyzer costs, the LCOH would increase. At 3.08 € per kg, their results are closer to our findings; however, they are still at a somewhat lower level. The cost range of 3.55–4.60 € per kg and 4.99–5.88 $ per kg, as

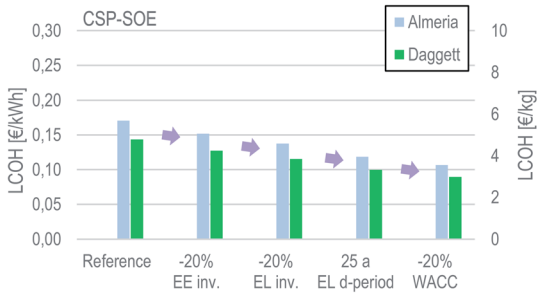

Fig. 14 Cost reduction potential of the CSP-SOE concept with the energy conversion efficiency unchanged.

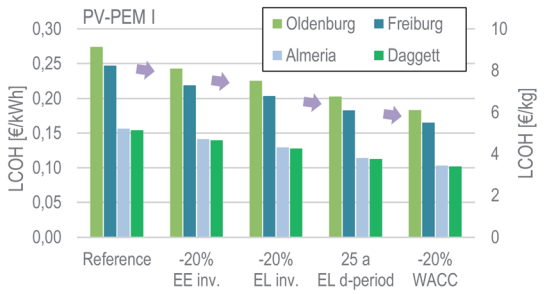

Fig. 15 Cost reduction potential of the PV-PEM I concept with the energy conversion efficiency unchanged.

presented by Heuser *et al.*[27] and Touili *et al.*,[28] respectively, are largely in agreement with the results from our study. As is shown in the literature overview, techno-economic analyses related to CSP-based hydrogen production concepts for direct comparison with our results are not available at present.

4 Conclusions

In this paper, candidate, utility-scale concepts of solar-based, electrolytic hydrogen production (solar-to-hydrogen, STH) were analyzed. On the power provision side, photovoltaic and concentrated solar power systems were considered. These options are combined with electrolytic hydrogen production alternatives of PEM electrolysis with (PV-PEM I and CSP-PEM) or without (PV-PEM II) power converters for electric coupling. Additionally, a concept including CSP and solid oxide electrolysis coupled *via* a power converter (CSP-SOE) has been considered for evaluating the effect of integrating heat from the CSP process into high-temperature electrolysis. A TRL analysis of the sub-components revealed that the highest pathway TRL levels can be estimated for the PV- and CSP-based power generation, coupled to a PEM electrolysis system, due to the high maturity of subsystems. Low TRL was found for systems comprising SOE technology. Photo-electrochemical water-splitting is not further explored within the model, as the low TRL of this technology does not promise near-term economic feasibility.

The developed techno-economic model was applied to determine hydrogen production volumes and the levelized cost of hydrogen (LCOH) at the locations of Oldenburg and Freiburg in Germany, as well as Almeria in Spain and Daggett in the USA, employing location-specific irradiation and ambient temperature data. Due to comparatively low irradiation levels in Germany, CSP-based systems have not been considered here. All cost data was projected for the reference year 2025.

The lowest LCOH of 14 €-ct per kW per h_{H_2} was found for the CSP-SOE and CSP-PEM pathways in Daggett. At reduced irradiation levels in Almeria, these pathways show an LCOH increase of 19%. The LCOH of the PEM-based pathways are slightly elevated, with values ranging from 15–16 €-ct per kW per h_{H_2} for both high-irradiance locations. For the two locations in Germany, the LCOH related to the PV-PEM concepts is 58–84% higher compared to the locations of Almeria and Daggett due to the considerably lower irradiation levels. Our analysis reveals that there is no significant cost effect of applying power converters for connecting PV modules and PEM electrolysis. We conclude that a theoretically increased hydrogen production volume through the employment of a power converter is not evident because the cost-optimization procedure leads to a lower electrolyzer capacity, which in turn reduces hydrogen production volumes. Furthermore, our analysis shows that the cost-competitiveness of CSP-EL compared to PV-PEM concepts increases with irradiation levels.

LCOH differences of CSP-SOE compared to CSP-PEM are found to be small and may be within computational error tolerances. However, CSP-SOE shows substantially higher hydrogen production levels of 36% relative to CSP-PEM at both of the locations considered. Hence, STH efficiencies are also highest, with 16–18%, at the locations of Almeria and Daggett.

The LCOH values achieved by the solar-to-hydrogen concepts considered in this study at the parameter settings chosen and with regard to an expected capital cost level in 2025 were still significantly higher than the DOE's 2020 targets for economically-viable hydrogen production of 6 $-ct per kW per h. However, if it was possible to further reduce component and capital costs by 20% and also achieve depreciation periods of 25 years for electrolyzers, the LCOH would range from 9–12 €-ct per kW per h_{H_2} for the high-irradiance locations and, thus, would be closer to the DOE targets.

In relation to future research, a further system optimization is suggested regarding the implementation of short-term energy storage, which might be particularly relevant at locations with higher fluctuations in power supply. Moreover, revenues from selling surplus electricity that is not consumed by the electrolyzer could improve the overall plant economics. However, local regulations on renewable power feed-in must be considered.

Abbreviations

a	Modified ideality factor
A_{EL}	Active electrode area of the electrolyzer
AM	Air mass
e	Elementary charge
EL	Electrolysis
G	Solar irradiation
G_{design}	Design irradiance

HER	Hydrogen evolution reaction
I_0	Diode reverse saturation current
I_{MPP}	Current at MPP
I_{ph}	Photo current
I_{SC}	Short circuit current
J_{nom}	Current density at nominal operating point of electrolyzer
LCOE	Levelized cost of electricity
LCOH	Levelized cost of hydrogen
MPP	Maximum power point of a photovoltaic module
NREL	National Renewable Energy Laboratory (USA)
OER	Oxygen evolution reaction
PEC	Photoelectrolysis
PEM	Polymer electrolyte membrane
Pt	Platinum
P_{MPP}	Power at MPP
PV	Photovoltaic
PV-EL	Coupled photovoltaic electrolysis system
U_{MPP}	Voltage at MPP
U_{nom}	Voltage at nominal operation point of electrolyzer
U_{OC}	Open circuit voltage
R_p	Shunt resistance
R_s	Series resistance
SAM	System advisor module
SHJ	Silicon heterojunction technology
STH	Solar-to-hydrogen
T_{amb}	Ambient temperature
T_{EL}	Electrolysis temperature
T_{PV}	Cell temperature of the PV subsystem
T_{op}	Operating temperature of the electrolyte
TiO_2	Titanium dioxide
η	Efficiency

Conflicts of interest

There are no conflicts of interest to be declared.

Acknowledgements

This work was supported by the Helmholtz Association under the Joint Initiative "EnergySystem 2050 – A Contribution of the Research Field Energy".

References

1 A. Otto, M. Robinius, T. Grube, S. Schiebahn, A. Praktiknjo and D. Stolten, Power-to-Steel: Reducing CO_2 Through the Integration of Renewable Energy and Hydrogen into the German Steel Industry, *Energies*, 2017, **10**(4), 451.

2 M. Robinius, A. Otto, P. Heuser, L. Welder, K. Syranidis, D. Ryberg, T. Grube, P. Markewitz, R. Peters and D. Stolten, Linking the Power and Transport Sectors—Part 1: The Principle of Sector Coupling, *Energies*, 2017, **10**(7), 956.

3 M. Robinius, A. Otto, K. Syranidis, D. S. Ryberg, P. Heuser, L. Welder, T. Grube, P. Markewitz, V. Tietze and D. Stolten, Linking the Power and Transport Sectors—Part 2: Modelling a Sector Coupling Scenario for Germany, *Energies*, 2017, **10**(7), 957.

4 M. Reuß, J. Reul, T. Grube, M. Langemann, S. Calnan, M. Robinius, R. Schlatmann, U. Rau and D. Stolten, Solar hydrogen production: a bottom-up analysis of different photovoltaic-electrolysis pathways, *Sustainable Energy Fuels*, 2019, **3**, 801–813, DOI: 10.1039/C9SE00007K.

5 R. E. Clarke, S. Giddey, F. T. Ciacchi, S. P. S. Badwal, B. Paul and J. Andrews, Direct coupling of an electrolyser to a solar PV system for generating hydrogen, *Int. J. Hydrogen Energy*, 2009, **34**(6), 2531–2542, DOI: 10.1016/j.ijhydene.2009.01.053.

6 S. M. S. Privitera, M. Muller, W. Zwaygardt, M. Carmo, R. G. Milazzo, P. Zani, M. Leonardi, F. Maita, A. Canino, M. Foti, F. Bizzarri, C. Gerardi and S. A. Lombardo, Highly efficient solar hydrogen production through the use of bifacial photovoltaics and membrane electrolysis, *J. Power Sources*, 2020, **473**, 228619, DOI: 10.1016/j.jpowsour.2020.228619.

7 S. Muhammad-Bashir, M. Al-Oufi, M. Al-Hakami, M. A. Nadeem, K. Mudiyanselage and H. Idriss, Comparison between the performance of high concentrated and non-concentrated PV-cells for hydrogen production using PEM water electrolyzers, *Sol. Energy*, 2020, **205**, 461–464, DOI: 10.1016/j.solener.2020.05.077.

8 J. Turner, G. Sverdrup, M. K. Mann, P.-C. Maness, B. Kroposki, M. Ghirardi, R. J. Evans and D. Blake, Renewable hydrogen production, *Int. J. Energy Res.*, 2008, **32**(5), 379–407, DOI: .

9 T. J. Jacobsson, V. Fjällström, M. Edoff and T. Edvinsson, Sustainable solar hydrogen production: from photoelectrochemical cells to PV-electrolyzers and back again, *Energy Environ. Sci.*, 2014, **7**, 2056.

10 I. Dincer and C. Acar, Review and evaluation of hydrogen production methods for better sustainability, *Int. J. Hydrogen Energy*, 2015, **40**(34), 11094–11111, DOI: 10.1016/j.ijhydene.2014.12.035.

11 C. Acar and I. Dincer, Comparative assessment of hydrogen production methods from renewable and non-renewable sources, *Int. J. Hydrogen Energy*, 2014, **39**(1), 1–12, DOI: 10.1016/j.ijhydene.2013.10.060.

12 I. Dincer, Green methods for hydrogen production, *Int. J. Hydrogen Energy*, 2012, **37**(2), 1954–1971, DOI: 10.1016/j.ijhydene.2011.03.173.

13 M. G. Kibria and Z. Mi, Artificial photosynthesis using metal/nonmetal-nitride semiconductors: current status, prospects, and challenges, *J. Mater. Chem. A*, 2016, **4**(8), 2801–2820, DOI: 10.1039/c5ta07364b.

14 F. Sayedin, A. Maroufmashat, R. Roshandel and S. S. Khavas, Optimal design and operation of a photovoltaic-electrolyser system using particle swarm optimisation, *Int. J. Sustain. Energy*, 2016, **35**(6), 566–582, DOI: 10.1080/14786451.2014.922974.

15 F. Sayedin, A. Maroufmashat, S. Al-Adwani, S. Sattari, A. Elkamel and M. Fowler, Evolutionary Optimization Approaches for Direct Coupling Photovoltaic-Electrolyzer Systems, *Industrial Engineering and Operations Management (IEOM), 2015 International Conference*, 2015.

16 F. Sayedin, A. Maroufmashat, S. Sattari, A. Elkamel and M. Fowler, Optimization of photovoltaic electrolyzer hybrid systems; taking into account the effect of climate conditions, *Energy Convers. Manage.*, 2016, **118**, 438–449, DOI: 10.1016/j.enconman.2016.04.021.
17 R. García-Valverde, N. Espinosa and A. Urbina, Optimized method for photovoltaic-water electrolyser direct coupling, *Int. J. Hydrogen Energy*, 2011, **36**(17), 10574–10586, DOI: 10.1016/j.ijhydene.2011.05.179.
18 R. García-Valverde, C. Miguel, R. Marténez-Béjar and A. Urbina, Optimized photovoltaic generator–water electrolyser coupling through a controlled DC–DC converter, *Int. J. Hydrogen Energy*, 2008, **33**(20), 5352–5362, DOI: 10.1016/j.ijhydene.2008.06.015.
19 Z. Su, S. Ding, Z. Gan and X. Yang, Analysis of a photovoltaic-electrolyser direct-coupling system with a V-trough concentrator, *Energy Convers. Manage.*, 2016, **108**, 400–410, DOI: 10.1016/j.enconman.2015.10.078.
20 S. Kirner, P. Bogdanoff, B. Stannowski, R. van de Krol, B. Rech and R. Schlatmann, Architectures for scalable integrated photo driven catalytic devices—a concept study, *Int. J. Hydrogen Energy*, 2016, **41**(45), 20823–20831, DOI: 10.1016/j.ijhydene.2016.05.088.
21 B. A. Pinaud, J. D. Benck, L. C. Seitz, A. J. Forman, Z. Chen, T. G. Deutsch, B. D. James, K. N. Baum, G. N. Baum, S. Ardo, H. Wang, E. Miller and T. F. Jaramillo, Technical and economic feasibility of centralized facilities for solar hydrogen production via photocatalysis and photoelectrochemistry, *Energy Environ. Sci.*, 2013, **6**(7), 1983–2002, DOI: 10.1039/C3EE40831K.
22 M. R. Shaner, H. A. Atwater, N. S. Lewis and E. W. McFarland, A comparative technoeconomic analysis of renewable hydrogen production using solar energy, *Energy Environ. Sci.*, 2016, **9**(7), 2354–2371, DOI: 10.1039/c5ee02573g.
23 M. Dumortier, S. Tembhurne and S. Haussener, Holistic design guidelines for solar hydrogen production by photo-electrochemical routes, *Energy Environ. Sci.*, 2015, **8**(12), 3614–3628, DOI: 10.1039/c5ee01821h.
24 M. Dumortier and S. Haussener, Design guidelines for concentrated photo-electrochemical water splitting devices based on energy and greenhouse gas yield ratios, *Energy Environ. Sci.*, 2015, **8**(11), 3069–3082, DOI: 10.1039/c5ee01269d.
25 M. Fasihi, D. Bogdanov and C. Breyer, Techno-Economic Assessment of Power-to-Liquids (PtL) Fuels Production and Global Trading Based on Hybrid PV-Wind Power Plants, *Energy Procedia*, 2016, **99**, 243–268, DOI: 10.1016/j.egypro.2016.10.115.
26 D. Teichmann, W. Arlt and P. Wasserscheid, Liquid organic hydrogen carriers as an efficient vector for the transport and storage of renewable energy, *Int. J. Hydrogen Energy*, 2012, **37**(23), 18118–18132, DOI: 10.1016/j.ijhydene.2012.08.066.
27 P. Heuser, T. Grube, H. Heinrichs, M. Robinius and D. Stolten, Worldwide Hydrogen Provision Scheme Based on Renewable Energy, Preprint 2020, 2020020100, 2020.
28 S. Touili, A. Alami Merrouni, A. Azouzoute, Y. El Hassouani and A.-i. Amrani, A technical and economical assessment of hydrogen production potential from solar energy in Morocco, *Int. J. Hydrogen Energy*, 2018, **43**(51), 22777–22796, DOI: 10.1016/j.ijhydene.2018.10.136.
29 R. Boudries, Techno-economic study of hydrogen production using CSP technology, *Int. J. Hydrogen Energy*, 2018, **43**(6), 3406–3417, DOI: 10.1016/j.ijhydene.2017.05.157.
30 Z. Wang, R. R. Roberts, G. F. Naterer and K. S. Gabriel, Comparison of thermochemical, electrolytic, photoelectrolytic and photochemical solar-to-hydrogen production technologies, *Int. J. Hydrogen Energy*, 2012, **37**(21), 16287–16301, DOI: 10.1016/j.ijhydene.2012.03.057.
31 M. Roeb, N. Monnerie, A. Houaijia, D. Thomey, and C. Sattler, Chapter 4 – Solar Thermal Water Splitting A2 – Gandía, Luis M, in *Renewable Hydrogen Technologies*, ed. G. Arzamendi and P.M. Diéguez, Elsevier, Amsterdam, 2013, pp. 63–86.
32 J. C. Mankins, *Technology Readiness Level*, 1995.
33 E.U., *Horizon 2020 – Work Programme*, 2014.
34 M. Kopp, D. Coleman, C. Stiller, K. Scheffer, J. Aichinger, B. Scheppat and E. Mainz, Technical and economic analysis of the worldwide largest power-to-gas plant with PEM electrolysis, *Int. J. Hydrogen Energy*, 2017, **42**(19), 13311–13320, DOI: 10.1016/j.ijhydene.2016.12.145.
35 *Power Tower Projects*, 2020, 19.08.2020, available from https://solarpaces.nrel.gov/by-technology/power-tower.
36 *Energy from the Desert: Very Large Scale PV Power Plants for Shifting to Renewable Energy Future*, 2015.
37 Air Liquide adds 20 MW hydrogen system to Bécancour plant, Press release 2019, 25.02.2019–19.08.2020, available from https://www.plant.ca/sustainability/air-liquide-adds-20-mw-hydrogen-system-to-becancour-plant-181614/.
38 C. Wulf, J. Linßen and P. Zapp, Review of Power-to-Gas Projects in Europe, *Energy Procedia*, 2018, **155**, 367–378, DOI: 10.1016/j.egypro.2018.11.041.
39 *Typical Meteorological Year Data*, European Commission and Joint Research Centre (JRC), 2017.
40 *System Advisor Model (SAM)*, National Renewable Energy Laboratory, Golden, CO, 2017.
41 V. Tamrakar, S. C. Gupta and Y. Sawle, Single-Diode and Two-Diode PV Cell Modeling Using Matlab for Studying Characteristics of Solar Cell Under Varying Conditions, *Electrical & Computer Engineering: An International Journal*, 2015, **4**(2), 67–77, DOI: 10.14810/ecij.2015.4207.
42 W. De Soto, S. A. Klein and W. A. Beckman, Improvement and validation of a model for photovoltaic array performance, *Sol. Energy*, 2006, **80**(1), 78–88, DOI: 10.1016/j.solener.2005.06.010.
43 R. I. Dunn, P. J. Hearps and M. N. Wright, Molten-Salt Power Towers: Newly Commercial Concentrating Solar Storage, *Proc. IEEE*, 2012, **100**(2), 504–515, DOI: 10.1109/JPROC.2011.2163739.
44 J. Dersch and S. Dieckmann, *Greenius – The Green Energy System Analysis Tool*, German Aerospace Center, Cologne, 2019.

45 NREL, *System Advisor Model (SAM)*, 2017, cited 2017, available from https://sam.nrel.gov/.
46 Q. Fang, L. Blum and N. H. Menzler, Performance and Degradation of Solid Oxide Electrolysis Cells in Stack, *J. Electrochem. Soc.*, 2015, **162**(8), F907–F912, DOI: 10.1149/2.0941508jes.
47 G. Tjarks, A. Gibelhaus, F. Lanzerath, M. Müller, A. Bardow and D. Stolten, Energetically-optimal PEM electrolyzer pressure in power-to-gas plants, *Appl. Energy*, 2018, **218**, 192–198, DOI: 10.1016/j.apenergy.2018.02.155.
48 S. Nordmann, B. Berghoff, A. Hessel, N. Wilck, B. Osullivan, M. Debucquoy, J. John, S. Starschich and J. Knoch, A monolithic all-silicon multi-junction solar device for direct water splitting, *Renewable Energy*, 2016, **94**, 90–95, DOI: 10.1016/j.renene.2016.03.050.
49 I. Fraunhofer, *Photovoltaics Report*, ISE Fraunhofer, 2017.
50 M. Bolinger, J. Seel and K. LaCommare, *Empirical Analysis of Project Cost, Performance, and Pricing*, Lawrence Berkeley National Laboratory, 2017.
51 D. Feldman, R. Margolis, M. Bolinger, D. Chung, R. Fu, J. Seel, G. Barbose, C. Davidson, N. Darghouth and R. Wiser, *Photovoltaic System Pricing Trends*, U.S Department of Energy, 2015.
52 J. Seel, G. Barbose and R. Wiser, *Why Are Residential PV Prices in Germany So Much Lower Than in the United States?*, Lawrence Berkeley National Laboratory, 2013.
53 *The Power to Change: Solar and Wind Cost Reduction Potential to 2025*, The International Renewable Energy Agency (IRENA), 2016.
54 S. Dieckmann, J. Dersch, S. Giuliano, M. Puppe, E. Lüpfert, K. Hennecke, R. Pitz-Paal, M. Taylor and P. Ralon. LCOE Reduction Potential of Parabolic Trough and Solar Tower CSP Technology until 2025, in *SolarPACES Conference*, DLR, Abu Dhabi, 2016.
55 T. Smolinka, M. Günther and J. Garche, *NOW-Studie: Stand und Entwicklungspotenzial der Wasserelektrolyse zur Herstellung von Wasserstoff aus regenerativen Energien*, Fraunhofer ISE, 2011.
56 L. Bertuccioli, A. Chan, D. Hart, F. Lehner, B. Madden and E. Standen, *Development of Water Electrolysis in the European Union – Final Report*, E4tech Sàrl/element energy, Lausanne/Cambridge, 2014.
57 S. M. Saba, M. Müller, M. Robinius and D. Stolten, The investment costs of electrolysis – a comparison of cost studies from the past 30 years, *Int. J. Hydrogen Energy*, 2018, **43**(3), 1209–1223, DOI: 10.1016/j.ijhydene.2017.11.115.
58 M. C. Jürgen Mergel and D. Fritz, Status on Technologies for Hydrogen Production by Water Electrolysis, in *Transition to Renewable Energy Systems*, 2013.
59 I. Fraunhofer, *PlanDelyKad: Studie über die Planung einer Demonstrationsanlage zur Wasserstoff-Kraftstoffgewinnung durch Elektrolyse mit Zwischenspeicherung in Salzkavernen unter Druck*, ISE Fraunhofer, Ludwig-Bölkow-Systemtechnik, DLR Stuttgart, 2014.
60 O. Schmidt, A. Gambhir, I. Staffell, A. Hawkes, J. Nelson and S. Few, Future cost and performance of water electrolysis: an expert elicitation study, *Int. J. Hydrogen Energy*, 2017, **42**(52), 30470–30492, DOI: 10.1016/j.ijhydene.2017.10.045.
61 *Prices of electricity for the industry in Germany from 2008 to 2018*, 22.04.2020, available from https://www.statista.com/statistics/595803/electricity-industry-price-germany/.

